Contents lists available at ScienceDirect

Microelectronic Engineering

Mechanical properties and fracture mechanism of porous SiOCH low-k dielectrics

H.L. Chang *, C.T. Kuo, M.S. Liang

Institution of Executive Master of Business Administration, National Chiao Tung University and Department of Material Science and Engineering, National Chiao Tung University, Taiwan

ARTICLE INFO

ABSTRACT

A series of low-k dielectric films with various mechanical properties were prepared for a 32-nm back-end-of-line technology node. Various precursors were used, and the porogen removal treatment was performed using the H_2 or E-beam-assisted method. This study presents a novel approach for determining the loss of materials during treatment. This approach includes determining yield strength, fracture toughness, bonding structure, and fracture mechanism of a series of low-k silica films. The results show that a low-k film formed using the precursor trimethylsilane has higher yield strength and fracture toughness than the low-k films formed using the precursor tetramethylsilane or octa-methylcyclotetrasiloxane. The residual gas analysis was conducted to determine the loss of materials and predict the bonding structure; the results show that the E-beam treatment rearranges the structure more effectively than the H_2 treatment by using the H radial to decompose the methyl group. Finally, the fracture mechanism of these low-k films was determined by relating the crack patterns of the indents on these films to their indentation load–displacement curves.

© 2011 Elsevier B.V. All rights reserved.

1. Introduction

As the feature sizes continue to shrink to improve their resis-tance–capacitance performance, porous low-k materials are used in their back-end-of-line (BEOL). Because low-k materials are mechanically weak, the post-process treatment is crucial for recon-structing the bonding and efficiently removing porogen. The fun-damental understanding of such treatment is important for controlling the treatment depth and the film properties. Because low-k materials are porous, determining their mechanical proper-ties is challenging. In general, a material fractures elastically under stresses much lower than its cohesive strength [1]. The discrep-ancy between the observed fracture strength and the theoretical cohesive strength was explained by the pioneering work of Griffith, who proposed that the propagation of cracks from defects or the cracking in the material by magnification of local stress concentra-tions causes the final fracturing [2]. Low-k materials are normally low in density, because pores were added to them to achieve low-k values. The degradation of mechanical properties caused by these defect-like intrinsic pores is the main concern in the applications of these low-k films as semiconductor BEOL interconnect technol-ogies, because such degradations may result in films peeling and cracking during processing. Mechanical properties such as yield strength and fracture toughness of thin-film/thick-substrate com-posites are difficult to measure using conventional techniques. This paper demonstrates an approach to measure these properties using a nanoindentation technique already used to measure the hardness and Young's modulus of thin films. This approach de-scribes a systematic relationship between a thin film and the thin film/substrate system [3]. The results of ductile/brittle behavior studies of various low-k films deposited on Si substrates suggest that great benefits can be gained in low-k film evaluation and development by using this approach.

2. Experiments

Six low-k films with k = 3.1, 2.75, 2.7, 2.6, 2.4, and 2.4, labeled as Samples 1–6, respectively, were deposited on Si wafers by plasma-enhanced chemical vapor deposition. Films were prepared using different precursors and post-treatments, as shown in Table 1. Sample 1 was prepared using the trimethylsilane (Si:C:O = 1:3:0) precursor and Sample 4 was prepared using the tetramethylsilane (4MS) (Si:C:O = 1:4:0) precursor. Samples 2 and 3 were prepared using the octamethylcyclotetrasiloxane (Si:C:O = 1:2:1) precursor, but Sample 3 had an additional He treatment applied to it. Samples 5 and 6 were prepared using the 4MS precursor with additional treatment by E-beam and H_2, respectively. All the ~600-nm-thick films were nanoindentation-tested to obtain their indentation curves by using a nanoindentor on a CSEM instrument with a force resolution of 1 μN and a displacement resolution of 0.3 nm. The

* Corresponding author. Tel.: +886 9 18610719.
  E-mail address: gladies.chang@gmail.com (H.L. Chang).

Table 1
Film characterization of Samples 1–6.

Sample	Precursor	Treatment	K
1	3MS		3.1
2	OMCTS		2.7
3	OMCTS	He	2.75
4	4MS		2.6
5	4MS	E-beam	2.4
6	4MS	H_2	2.4

corresponding indent marks were investigated by an atomic force microscope (AFM).

3. Results and discussion

Indentation curves are well known to specify the relationship between load P and displacement h, which are continuously monitored and recorded during indentation. From the indentation curve, hardness is defined as the peak load divided by the projected contact area, and Young's modulus is defined as the initial slope of the unloading part of the indentation curve. Fig. 1(a)–(d) shows the measured hardness and Young's modulus as a function of the indentation depth/film thickness for Samples 1–4, as calculated from their indentation curves with various test loads, with examples shown in Fig. 2(a)–(d).

The elastic/plastic deformation zone in a thin film/substrate composite produced by indentation expands to the substrate as the indent goes deeper into the thin film. Beyond a certain depth, hardness measurements are affected by not only film properties but also substrate properties. Thin film/substrate composites have been studied by a finite-element method to characterize their elastic–plastic response [4]. In the case of a soft film on a harder substrate, similar to the case considered in this study, the film's hardness can be described as

$$\frac{H}{H_s} = 1 + \left[\frac{H_f}{H_s} - 1\right] \exp\left[-\frac{(\sigma_f/\sigma_s)}{(E_f/E_s)}(h_c/t_f)^2\right], \tag{1}$$

where t_f is the film thickness, h_c is the contact depth, E is Young's modulus, σ is the yield strength, H is the hardness, and the subscripts f and s represent the film and the substrate, respectively, whereas no subscript represents the composite system. From Fig. 1(a)–(d) and Eq. (1), the yield strength values of Samples 1–4 are calculated to be 478, 52, 13, and 6.2 MPa, respectively. Under the same applied load, a film with higher yield strength has a smaller deformation zone compared to the one with lower yield strength. A soft low-k film exhibits low yield strength, indicating its tendency for brittle fracture under an applied stress. This suggests that for films with higher yield strength, the intrinsic film hardness can be measured at greater depths in bulk films, as demonstrated in the measured hardness depth profiles of Samples 1–4 shown in Fig. 1(a)–(d), with the lengths of the marked "A" plateaus corresponding to the intrinsic film hardness, in proportion to the film yield strength just calculated. Consequently, the intrinsic hardness values of Samples 1–4, which are independent of substrate properties, are measured at indentation depths of less than 40%, 35%, 30%, and 30% of the film thickness; these hardness values are found to be 2.137, 0.665, 0.601, and 0.453 GPa, respectively, as specified by the marked "A" plateaus in Fig. 1(a)–(d).

Nanoindentation tests on Sample 1 at peak indentation loads of 1, 2.5, and 5 mN yielded the smooth indentation curves in Fig. 2(a). The yield strength value indicates the applied stress at which the material begins to deform plastically; the yield strength varies for Samples 1–4. No cracking was detected by inspection with an
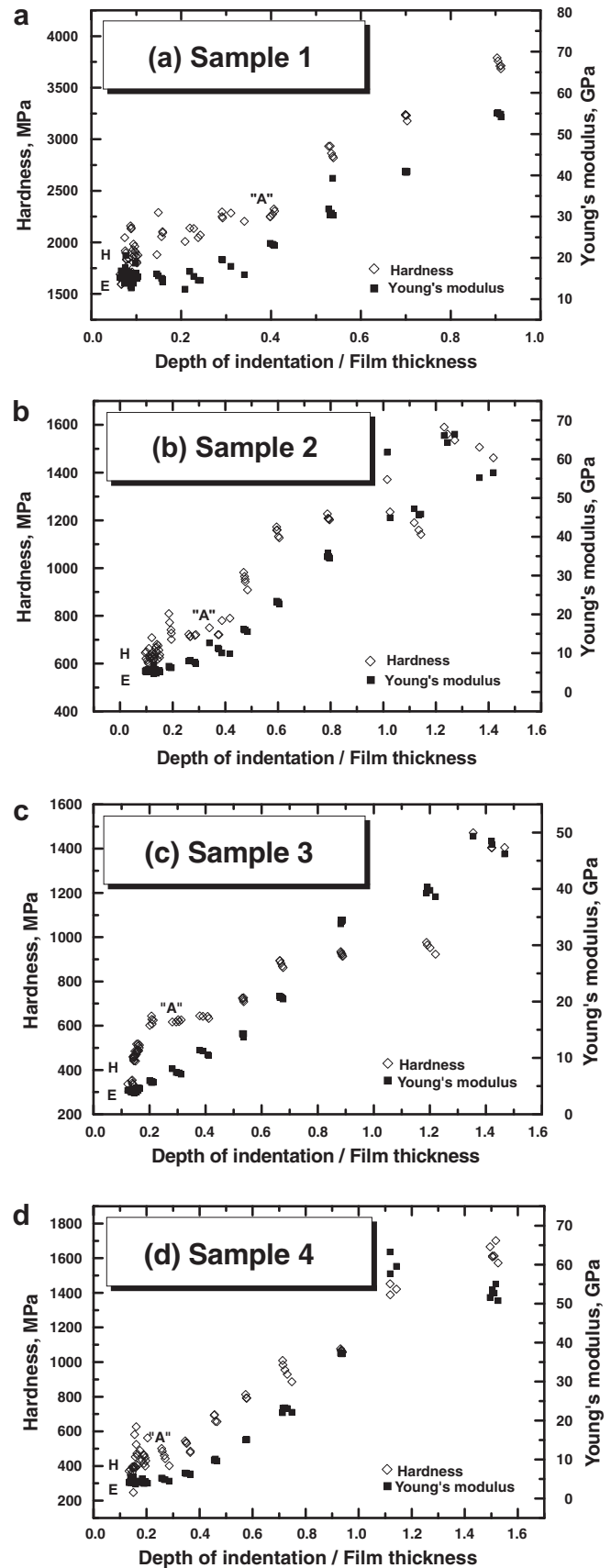

Fig. 1. (a)–(d) Hardness and Young's modulus as the function of depth/film thickness of Samples 1–4.
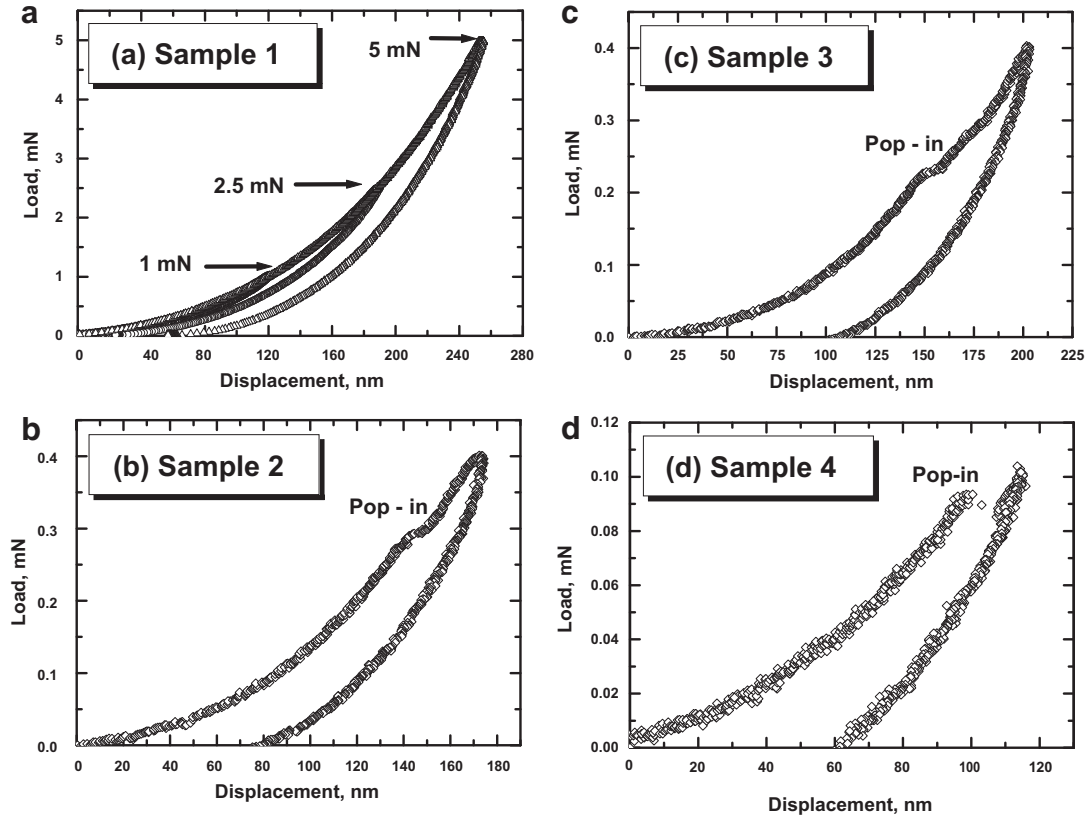
Fig. 2. (a)–(d) Indentation curves of Samples 1–4, with the first "pop in" for Samples 2–4 indicated in (b)–(d).
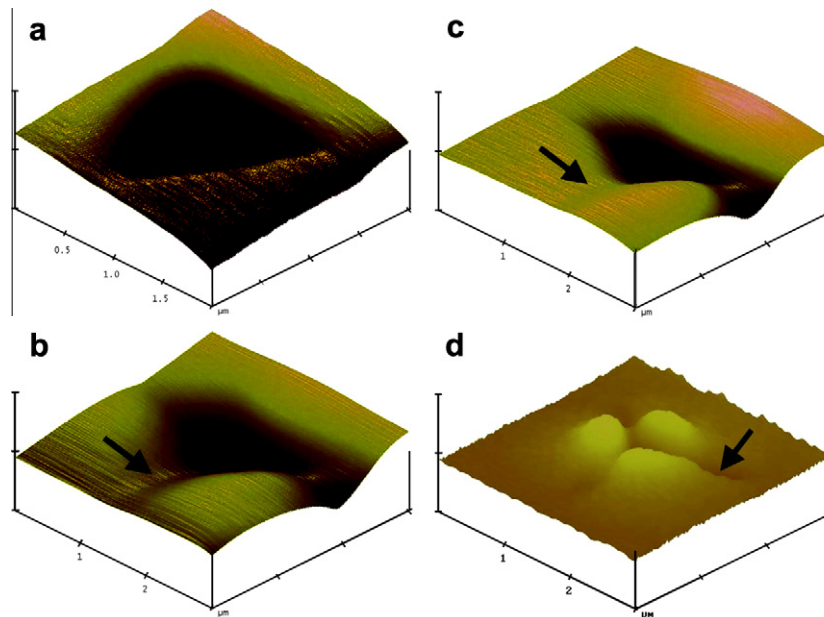

Fig. 3. (a)–(d) Corresponding indent mark AFM images to the indentation curves shown in Fig. 2(a)–(d) with arrows indicating the radial cracks at the edge of indent marks.

AFM for the maximum load of 5 mN; Fig. 3(a) reveals that Sample 1 underwent plastic deformation without cracking in the test load range of 1–5 mN. However, the indentation curves of Samples 2–4 under various test loads indicate sudden advances of the indenter tip into the materials, which are called "pop-in" kinks. Discontinuities in the indentation curves of Samples 2–4 at the first "pop-in" kinks were located at 0.3, 0.24, and 0.09 mN, respectively,

as shown in Fig. 2(b)–(d). The AFM images of Samples 2 and 3 shown in Fig. 3(b) and (c), respectively, reveal that these two films budged slightly upward and that radial cracks appeared at the edge of the indent marks. The AFM image of Sample 4 shown in Fig. 3(d) reveals that the film moved significantly upward and that radial cracks appeared at the edge of the indent mark. Because the indentation depths at which the "pop-in" kinks occurred are substan-
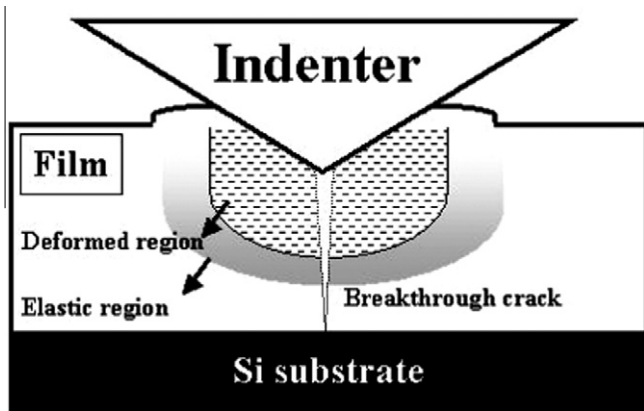
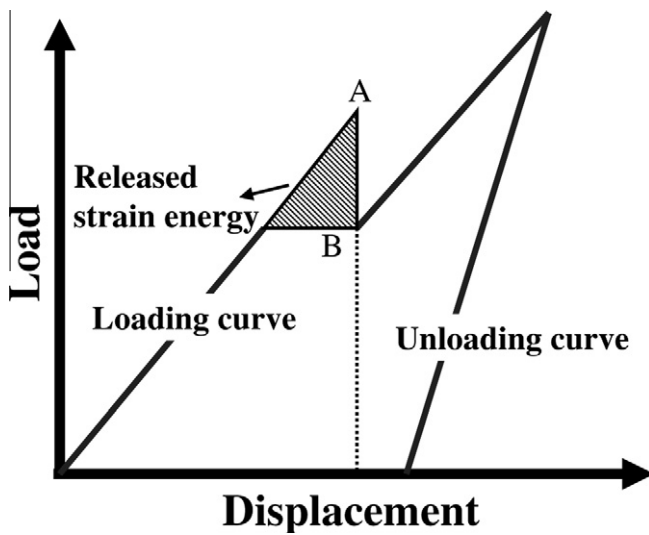**Fig. 4.** Schematic diagram of breakthrough crack formation.

Fig. 5. Schematic diagram of the released strain energy.

Table 2
Mechanical properties of Samples 1–6.

Sample	Hardness, Gpa	Young's modulus, Gpa	Yield strength, MPa	Fracture toughness (MPa m$^{1/2}$)
1	2.137	23.11	478	–
2	0.665	12.1	52	0.045
3	0.601	7.01	13	0.026
4	0.453	4.15	6.2	0.0049
5	1.72	18.01	–	–
6	1.50	16.50	–	–

tially less than the thickness and hardness of the films, and the Young's modulus of the Si substrate is much higher than those of the films, the kinks observed in Fig. 2(b)–(d) must result from the cracks in the films themselves rather than from cracks at the film/substrate interfaces or in the Si substrates.

The presence of a kink in the indentation curve is associated with the formation of a breakthrough crack in the film, schematically depicted in Fig. 4. A breakthrough crack in the film allows the indenter to be displaced farther without increasing the applied load. According to this breakthrough crack formation model, the released strain energy that is required to form a new crack surface can be determined using the specific area projected by the inden-
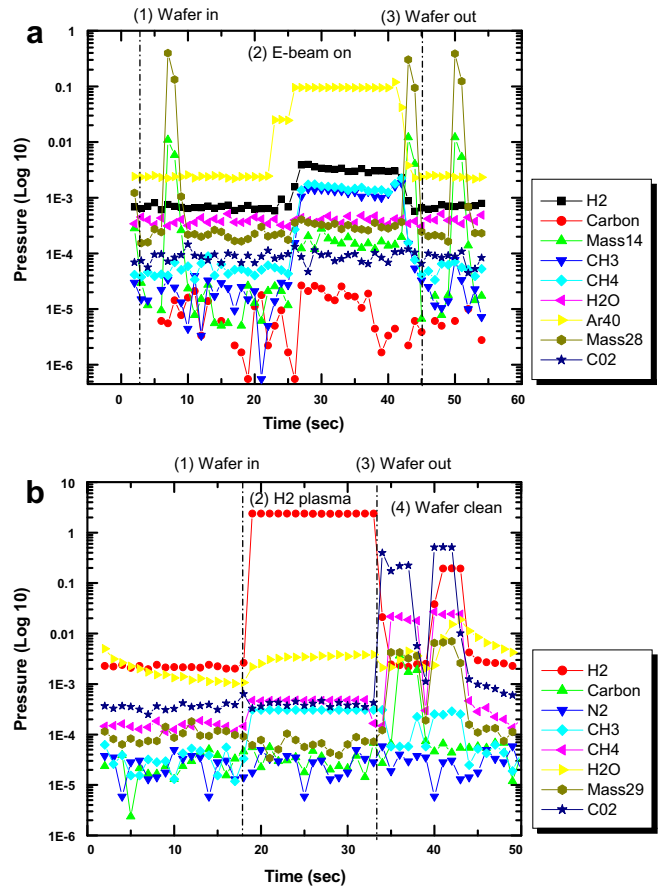

Fig. 6. (a) RGA spectrum of the E-beam treated low-k. (b) RGA spectrum of the H$_2$ treated low-k.

tation curve, as first proposed by Li et al. [5]. The fracture of the films under load-controlled indentation can be observed in the load–displacement curve shown in Fig. 5. When a brittle film yields, a crack is generated to release high strain, which is indicated by the shadowed region in Fig. 5. The behavior of the applied load and the displacement changes when a crack is generated; the AB segment (Fig. 5) represents the drop in load strength when an internal crack is generated.

As mode I fracture is dominant, the opening mode in plane strain, the critical stress-intensity factor or the fracture toughness, K_{IC}, can be written as

$$K_{IC} = \left[\frac{EG}{(1 - v^2)}\right]^{1/2} \equiv \left[\frac{E}{(1 - v^2)2\pi CR}\left(\frac{U}{t}\right)\right]^{1/2}$$

and

$$G = \left(\frac{1}{2\pi CR}\right)\left(\frac{dU}{dC}\right) \tag{2}$$

where E is the elastic modulus, G is the strain energy release rate, v is Poisson's ratio, C_R is the crack length in the film plane, and U is assessed from the kink. Based on Eq. (2), the calculated fracture toughness values are 0.045 MPa m$^{1/2}$, 0.026 MPa m$^{1/2}$, and 0.0049 MPa m$^{1/2}$ for Samples 2, 3, and 4, respectively. The fracture toughness for Sample 1 is not available, because it underwent plastic deformation for the entire load range. The mechanical properties of the films were measured by the nanoindentation technique and are summarized in Table 2.

Because Sample 4 has the lowest hardness and yield strength, treatments to improve its mechanical strength were studied. Samples 5 and 6 were formed using the same precursor as Sample 4,
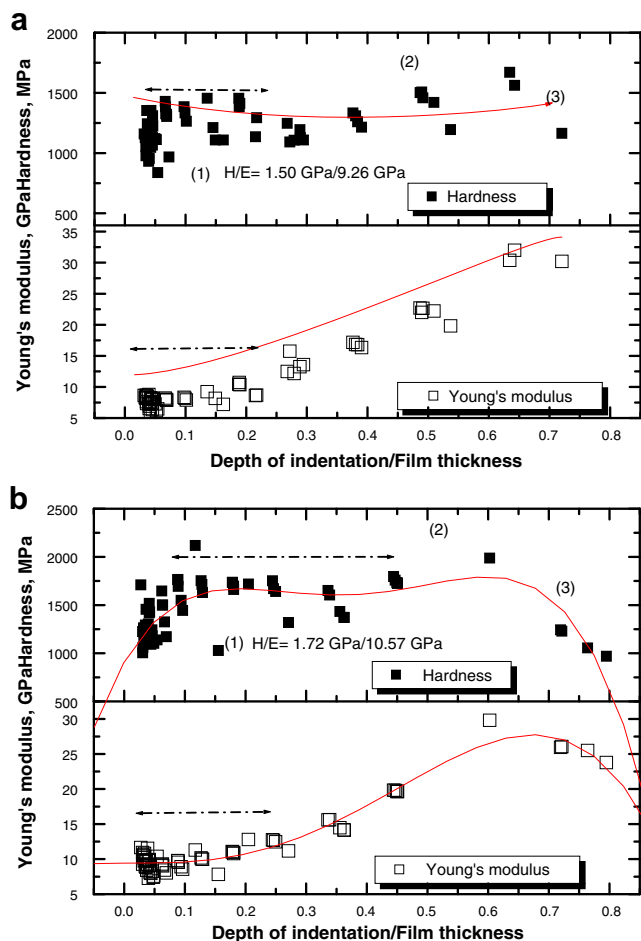
Fig. 7. (a) Hardness and Young's modulus of Sample 5.(b) Hardness and Young's modulus of Sample 6.

Fig. 8. (a) FTIR spectrum of Sample 5 before and after treatment. (b) Bonding structure change after treatment.

but then followed by the E-beam treatment for Sample 5 and the H_2 treatment for Sample 6. Fig. 6a and b presents residual gas analysis (RGA) spectra of Samples 5 and 6, respectively, following their post-treatments. Fig. 6a shows the three stages typical of RGA spectra of films with E-beam post-treatment: (1) the wafer processing stage, which corresponds to the wafer being moved in and out of the chamber; (2) the E-beam activation stage, which corresponds to the E-beam being turned on after the chamber pressure is stabilized; and (3) the methyl/methane group stage, which corresponds to when the methyl/methane group can be detected once the film is under the E-beam treatment. Similar behavior is observed for the film under H_2 treatment. To summarize, methyl/methane groups are the main byproducts of the E-beam treatment, and H_2 outgassing is the main byproduct of the H_2 treatment. The E-beam treatment causes the loss of 10 times as many methyl groups as the H_2 treatment, indicating that the E-beam treatment causes greater structural rearrangement.

To further study the mechanical properties of Samples 5 and 6, Fig. 7a and b presents their hardnesses and Young's modulus. The greater hardness following the E-beam treatment (1.72 GPa) than that following the H_2 treatment (1.5 GPa) is consistent with the analysis of the RGA spectra of Fig. 6a and b, which suggests that the E-beam treatment causes greater structural rearrangement than the H_2 treatment. FTIR bonding identification reveals that new Si–CH$_2$–Si bonds are formed and Si–CH$_3$ bonds are eliminated.

Fig. 8a shows the FTIR spectra of Sample 5 before and after the E-beam treatment. Fig. 8b is the subtraction curve derived from
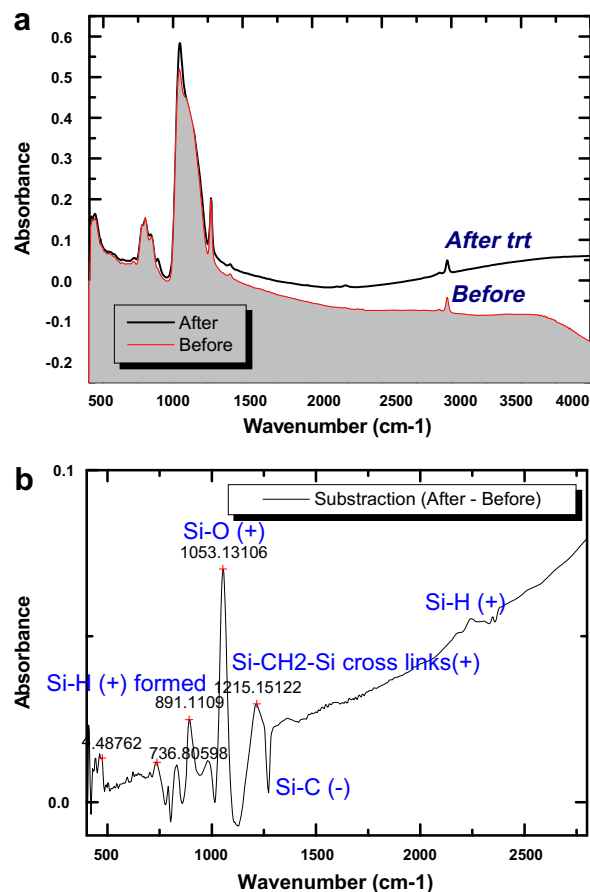
Fig. 8a to study the change in the bonding structure after the treatment. The treatment mechanism is considered a chain reaction between H radials and methyl groups. The dissociation of terminal bonds in Si–CH$_3$ by the formation of CH$_3$·H (methane) can change the bonding structure by forming new Si–CH$_2$–Si bonds. The Si–CH$_2$–Si network in the low k skeleton in Fig. 8b is considered to favor bonding that strengthens low-k films.

4. Conclusions

An approach based on indentation is developed to measure the mechanical properties of low-k films. Yield strength and fracture toughness, the most critical mechanical properties of low-k films in semiconductor processing were measured and compared. Chemical reactive treatments of low-k films that favor new bond formation to improve mechanical properties were also purposed. Tremendous benefits can be gained in low-k film evaluation for better film nature understanding and key indices can be identified and measured in film development for expedited process optimization, which greatly shorten the cycle time in delivering integration compatible low-k films.

References

[1] K.M. Lin, H.L. Chang, Mater. Sci. Eng. A 187 (1997) 139.
[2] G.D. Dieter, Mechanical Metallurgy, McGraw-Hill, London, 1988. pp. 241–272.
[3] H.L. Chang, C.T. Kuo, Dia. Relat. Mater. 10 (2001) 1910.
[4] B. Bhushan, Handbook of Micro/Nano Tribology, CRC, Bota Raton, 1995. pp. 434–525.
[5] X. Li, D. Diao, B. Bhushan, Acta Mater. 45 (1997) 4453.